An experiment to test centrifugal confinement for fusion*

R. F. Ellis, A. B. Hassam,† S. Messer, and B. R. Osborn
Department of Physics, University of Maryland, College Park, Maryland 20742

(Received 20 October 2000; accepted 21 December 2000)

The basic idea of centrifugal confinement is to use centrifugal forces from supersonic rotation to augment conventional magnetic confinement. Optimizing this ''knob'' results in a fusion device that features four advantages: steady state, no disruptions, superior cross-field confinement, and a simpler coil configuration. The idea rests on two prongs: first, centrifugal forces can confine plasmas to desired regions of shaped magnetic fields; second, the accompanying large velocity shear can stabilize even magnetohydrodynamic (MHD) instabilities. A third feature is that the velocity shear also viscously heats the plasma; no auxiliary heating is necessary to reach fusion temperatures. Regarding transport, the velocity shear can also quell microturbulence, leading to fully classical confinement, as there are no neoclassical effects. Classical parallel electron transport then sets the confinement time. These losses are minimized by a large Pastukhov factor resulting from the deep centrifugal potential well: at Mach 4–5, the Lawson criterion is accessible. One key issue is whether velocity shear will be sufficient by itself to stabilize MHD interchanges. Numerical simulations indicate that laminar equilibria can be obtained at Mach numbers of 4–5 but that the progression toward laminarity with increasing Mach number is accompanied by residual convection from the interchanges. The central goal of the Maryland Centrifugal Torus (MCT) [R. F. Ellis *et al.*, Bull. Am. Phys. Soc. **44**, 48 (1998)] is to obtain MHD stability from velocity shear. As an assist to accessing laminarity, MCT will incorporate two unique features: plasma elongation and toroidal magnetic field. The former raises velocity shear efficiency, and modest magnetic shear should suppress residual convection. [DOI: 10.1063/1.1350957]

I. INTRODUCTION

The basic idea of centrifugal confinement is to use centrifugal forces from rapid plasma rotation to augment conventional magnetic confinement.[1–4] In this sense, plasma rotation represents an additional ''knob'' that can be optimized to result in a fusion device that has several advantages.

Two factors motivate pursuit of this idea: first, the centrifugal forces constitute a ''gravitational force'' that can actually contain plasma, even along ''open'' field lines; second, the large velocity shear associated with the rotation can stabilize not only microinstability but possibly also macro-, magnetohydrodynamic (MHD) instabilities.

In Fig. 1, we depict the basic concept (a review article on rotating plasma devices is provided by Lehnert[2]). A poloidal magnetic field line with curvature is shown in axisymmetric geometry. If the plasma and the frozen-in field line are rotating toroidally, a fluid element (or a guiding center) experiences a radially outward centrifugal force. The component of this force perpendicular to the field lines is easily taken up by magnetic forces; the parallel component is unbalanced and tends to restore plasma to the midplane. The latter fact is expressed by the fluid equation

$$\mathbf{B}\cdot\nabla p = -nM\mathbf{B}\cdot(\mathbf{u}\cdot\nabla\mathbf{u}). \tag{1}$$

Unlike conventional magnetic confinement schemes where the pressure along the field lines would be constant ($\mathbf{B}\cdot\nabla p = 0$), here the inertial forces are large enough that the pressure can be contained to desired portions of the field lines by appropriate shaping. From a guiding center viewpoint this is analogous to a bead on a rotating wire.

A comparison of the two terms of Eq. (1) reveals that in order to attain significant pressure confinement, the flows must be supersonic. Thus, a key requirement of centrifugally confined schemes must be $M_s \gg 1$, where M_s is the sonic Mach number.

The experimental essentials of the centrifugal confinement scheme are summarized schematically for a particular configuration in Fig. 2. In this realization, the main magnetic field is a straight solenoid with axisymmetric mirror-like geometry at the ends. There is a cylindrical, conducting core that is electrically insulated from the outer vacuum wall. A radial electric field is applied by biasing the inner core at high voltage with respect to the outer wall. The electric field causes a plasma in the annulus to rotate azimuthally in $\mathbf{E}\times\mathbf{B}$ motion. The plasma is confined by centrifugal forces to the straight solenoid portion of the magnetic field. Note that the magnetic mirror force plays a negligible role in the confinement: without the centrifugal force, the mirror geometry has the usual conical loss cone in velocity space, but, for large Mach number rotation, this loss cone is almost completely closed because of the favorable centrifugal potential.

In what follows, we discuss guiding center orbits, MHD equilibrium, momentum and heat transport, and MHD stability, and show that the scheme is viable as a fusion device in that it exhibits the requisite confinement, heating, and stability properties. In particular, we show that the system can be

*Paper MI2 6, Bull. Am. Phys. Soc. **45**, 217 (2000).
†Invited speaker.

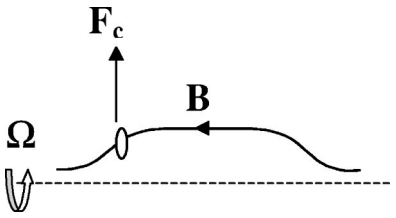

FIG. 1. An axisymmetric poloidal magnetic field line with a toroidally rotating fluid element depicting a radially outward centrifugal force.

scaled, with reasonable assumptions, to a reactor and that the resulting device has at least four advantages over tokamak reactors. An experiment, the Maryland Centrifugal Torus (MCT),[5] is planned to test the equilibrium and stability aspects of centrifugal confinement. We describe this in the final section.

In the discussion in this paper, the Mach number of the toroidal flow plays an important role. For reference, we define the Mach number, M_s, as $M_s \equiv u_T/(T/M)^{1/2}$, where u_T is the toroidal speed, T is the ion temperature, and M is the ion mass.

II. THEORETICAL BASIS

A. Particle orbits

The system is strongly magnetized, i.e., the Larmor radii are small. Thus, particle orbits can be analyzed in the drift approximation. The drift Hamiltonian, to lowest order in the small Larmor radius, is

$$H=(1/2)Mv_{\|}^2+\mu B-(1/2)MR^2\Omega^2. \tag{2}$$

Standard notation is used: R is the radial coordinate of a cylindrical (R,ζ,z) coordinate system, $v_{\|}$ is the speed along the field, μ is the magnetic moment of the guiding center, and Ω is the frequency of toroidal rotation. The axisymmetric magnetic field is described in the usual fashion by

$$\mathbf{B}=\nabla\zeta\times\nabla\psi+RB_T\nabla\zeta. \tag{3}$$

This Hamiltonian is derived assuming that the dominant particle drifts are the parallel motion and the $\mathbf{E}\times\mathbf{B}$ drift. In addition, the electric potential, ϕ, is approximately constant along a magnetic flux contour ψ and Ω and ϕ are related by $d\phi/d\psi\equiv\Omega$ (see Sec. II B).

Noting that $\mu\equiv Mv_{\perp}^2/B$, a comparison of the magnetic moment force and the centrifugal force potential in (2) reveals that for large Mach numbers the magnetic mirror potential can be neglected. The remaining Hamiltonian is that of a bead on a wire: the orbits are centered about the maximum R and bounce about that point centrifugally confined. For large Mach number, the excursion of the bounce from the maximum radius, ΔR, can be calculated to be $\Delta R/R \approx 1/M_s^2$.

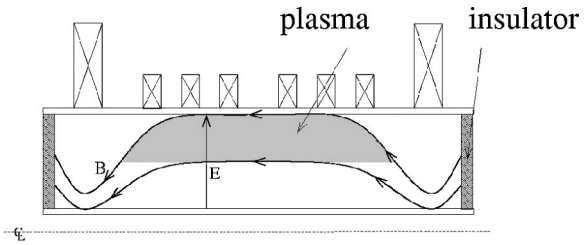

FIG. 2. Experimental schematic of one particular realization of a centrifugal confinement scheme.

To higher order, the gradient-B and curvature drifts need to be included in the Hamiltonian. For $B_T=0$, these drifts are in the toroidal direction and the above description does not change substantially—in particular, since the drifts are toroidal, there are no banana orbits. This is an important result since it implies that the classical transport in this system will not have any geometric, ''neoclassical'' enhancements. If $B_T\neq 0$, the particle orbits to lowest order are still just the bounce orbits described above, except that the motion also has a toroidally in–out component as the ''bead'' slides along the twisted wire. When gradient-B and curvature drifts are added, this introduces banana broadening. The width of the banana can be estimated to be of order $\rho(B_T/B)\times(1/M_s^2)$, where ρ is the gyroradius. Thus, unless B_T is very strong, the banana width is smaller than a gyroradius.

B. MHD equilibrium

For centrifugal confinement, the governing ideal MHD equilibrium equation also includes inertial forces, viz.,[2,4,6]

$$nM\mathbf{u}\cdot\nabla\mathbf{u}=-\nabla p+\mathbf{j}\times\mathbf{B}, \tag{4}$$

where the electrostatic potential ϕ and the flow $\mathbf{u}$ are related by

$$\nabla\phi=\mathbf{u}\times\mathbf{B}. \tag{5}$$

We use the representation for $\mathbf{B}$ given above. From (5), we note that $\mathbf{B}\cdot\nabla\phi=0$; assuming that the flow is toroidal, the perpendicular component of (5) gives

$$\mathbf{u}=R^2\Omega\nabla\zeta, \tag{6}$$

with $\Omega(\psi)\equiv d\phi/d\psi$. Thus, each field line rotates as a rigid rotor.

We now calculate that $\mathbf{u}\cdot\nabla\mathbf{u}=\Omega^2\nabla R^2/2$. Then, the toroidal component of Eq. (4) yields the condition

$$RB_T=I(\psi), \tag{7}$$

the component perpendicular to the field yields the counterpart to the Grad–Shafranov equation,[2,7,6]

$$\nabla\cdot(R^{-2}\nabla\psi)=IdI/d\psi+\partial p/\partial\psi+(1/2)nM\Omega^2\partial R^2/\partial\psi, \tag{8}$$

where $\partial/\partial\psi\equiv(RB)^{-2}\nabla\psi\cdot\nabla$, and the component parallel to the field yields

$$\mathbf{B}\cdot\nabla p=(1/2)nM\mathbf{B}\cdot\nabla(R^2\Omega^2). \tag{9}$$

The toroidal rotation speed, $u_T\equiv R\Omega$, in a centrifugal confinement scheme must satisfy the inequalities

$$c_s\ll u_T<V_{\mathrm{A}}, \tag{10}$$

that is to say the speed should be supersonic but sub-Alfvénic. Here, $c_s\equiv(T/M)^{1/2}$ is the sound speed and V_{A} is the Alfvén speed. The former inequality ensures large Mach number and parallel containment; the latter ensures that magnetic distortions are not large. Based on this ordering, the pressure term in (8) is negligible and the centrifugal terms

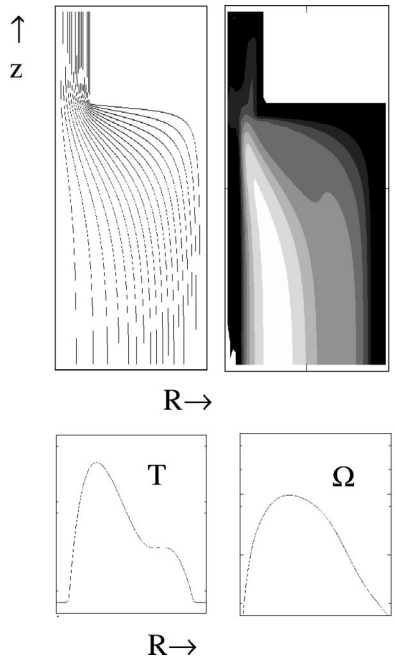

FIG. 3. Two-dimensional numerical MHD simulation demonstrating centrifugal confinement and concomitant viscous heating. Flux surfaces, pressure contours, and cuts of angular frequency and temperature are shown. The range of the major radius R, normalized, is $R=[0.2,1.2]$; that of z is $z=[0,2]$. Arbitrary units are used for the abscissas of the T and Ω plots.

distort the field lines by an amount of $O(u_T^2/V_A^2)$. The parallel force balance equation (9) demonstrates centrifugal confinement, as mentioned in the Introduction. To solve for the pressure in (9), we need the temperature distribution $T(R,\psi)$. The latter comes from the heat balance transport equation. As a simple limit, suppose $T=$const: in this case, the pressure can be solved for from (9) and is given by [2,4]

$$p(R,\psi)=p_0(\psi)\exp(MR^2/\Omega^2/4T). \tag{11}$$

The pressure drops off exponentially along a field line from the point of maximum radius. The exponential scale ΔR decreases with increasing Mach number as R/M_s^2, as given in Sec. II A. In the more general case, the temperature drops away from the peak pressure point toward the insulators; thus, the exponential pressure drop-off scale is set by the peak temperature but gets shorter as the temperature drops toward the insulators.

A two-dimensional (2-D) MHD numerical simulation was run to test the equilibrium aspects of centrifugal confinement.[8] The complete ideal MHD equations were solved in 2-D cylindrically axisymmetric geometry. The code also includes small amounts of constant resistivity, viscosity, and parallel and cross-field thermal conduction.

A contour plot of ψ, representing the field lines, is shown as the first clockwise plot of Fig. 3 (we show the cylindrical R-z cross section with reflection symmetry about $z=0$). This is a steady-state equilibrium, relaxed with respect to transport. We ran toroidal rotations with Mach numbers of up to 3. More than 90% of the currents are externally generated; the cross-field ''leakage'' currents and the diamagnetic currents from the thermal pressure and the rotation kinetic energy, make up the remaining currents—thus the flux plot is almost as it is in vacuum.

In the second clockwise plot of Fig. 3, we show a corresponding plot of the pressure contours. Centrifugal confinement is clearly evident. In the third clockwise plot, we show a cut along the $z=0$ axis of the angular frequency of toroidal rotation. The angular frequency was found to be almost a flux function, as expected. We also show a cut of the temperature in the fourth clockwise plot.

This equilibrium was generated by biasing the inner wall with respect to the outer wall. Insulating boundary conditions were used at the top and the bottom. Currents were fed into the plates to maintain the required potential difference against ''leakage'' currents from the viscosity and friction with neutrals.

This code was also rerun including an initial vacuum toroidal magnetic field from currents in the central core, of the order of the poloidal field. Practically the same equilibrium as above was obtained, as expected from the theory. The net flow was toroidal, vectorially made up of parallel flow and $\mathbf{E}\times\mathbf{B}$ perpendicular flow.

C. Transport

In an ideal plasma, any initial $\mathbf{E}\times\mathbf{B}$ flow would continue unabated. Transport processes—viscosity with coupling to the walls and friction with background neutrals—would, however, damp this motion on the long time scale (compared to MHD time scales). From a particle viewpoint, these retarding forces would result in Force$\times B$ drifts that would neutralize the charge between the inner and outer electrodes, thus lowering the electric field. To maintain the electric field, charge would have to be supplied to the plates by external circuits—the $I\times B$ forces from the external currents are indeed the forces[9] that are transmitted to the plasma to maintain the flow rate. This balance can be summarized by the equation

$$NMu_T^2/\tau_{\rm mom}=IV_0 \tag{12}$$

where $N\equiv n\times Volume$, I is the external current, V_0 is the applied voltage, and $\tau_{\rm mom}$ is the momentum confinement time from viscosity, charge exchange friction, etc. IV_0 is the input power to the plasma, $P_{\rm in}$.

The power dissipated in viscous processes and friction ends up as heat. If we assume that a fraction f_H of the input power ends up as heat, the heat balance equation in steady state can be written as

$$3NT/\tau_{\rm heat}=f_HIV_0-P_{\rm rad}, \tag{13}$$

where $\tau_{\rm heat}$ is the heat confinement time, and $P_{\rm rad}$ is the radiated power.

We take the confinement times to be as follows:

$$1/\tau_{\rm mom}=1/\tau_{\rm CX}+1/\tau_{\perp,i}+1/\tau_{\parallel,i}, \tag{14}$$

$$1/\tau_{\rm heat}=1/\tau_{\rm CX}+1/\tau_{\perp,i}+1/\tau_{\parallel,e}, \tag{15}$$

Here, $\tau_{\rm CX}$ represents the loss due to charge exchange with neutrals.[10] Charge exchange losses apply equally to momentum and heat. The remaining losses can be separated accord-

ing to losses perpendicular to and parallel to the magnetic field. The perpendicular losses are represented by $\tau_{\perp,i}$. For our model, we take these to be classical on the grounds that the large velocity shear in the system will suppress microturbulence. In this case, the cross-field viscosity and thermal conductivity from Braginskii[11] can be seen to be dominated by the ions and both have diffusivities of order $\rho_i^2 \nu_{ii}$. Thus,

$$\tau_{\perp,i} \sim a^2/(\rho_i^2 \nu_{ii}). \tag{16}$$

The parallel particle and heat losses to the insulators, along the magnetic field, can be assessed as follows.[4] For high Mach numbers, the ions are very tightly confined, as was discussed in Sec. II A. Nonetheless, energetic ions on the very tail of the distribution may escape the centrifugal potential well. This leads to particle and momentum loss. Once these ions are lost, more losses are incurred only if ions are scattered into this exponentially small loss cone by ion–ion collisions. This loss occurs at the ion–ion collision rate based on the energetic ions; in addition, the number of energetic ions is exponentially small for a Maxwellian distribution. The resulting loss rate is of order $\nu_{ii}/[(M_s^2/4)\exp(M_s^2/4)]$, where the mitigating factor containing M_s^2 terms is the well-known Pastukhov factor[12] which results from the deep centrifugal potential well as well as an electrostatic potential well (discussed further below). This is the rate for parallel particle and momentum loss.

The lighter electrons are not centrifugally confined. However, their tendency to escape is arrested by a space charge electrostatic potential build up along a field line. The electron particle loss rate is equal to the ion loss rate as above. The heat loss rate, however, is larger and the more important concern here:[4] energetic electrons can reach the insulators, transfer heat, and return as cold electrons. The parallel electron heat loss is thus based on ν_{ee} and scales as

$$\tau_{\parallel,e} \sim (1/\nu_{ee})(M_s^2/4)\exp(M_s^2/4). \tag{17}$$

The Pastukhov factor again applies since the self-consistent electric potential well, $e\phi/T$, is deep and scales as the square of the Mach number. Note that this well is deeper than for classical mirrors[12] and, to an extent, controllable.

The electron heat loss along the field is the one that would limit the energy confinement time in a reactor. For $n\tau_{\parallel,e}$ based on (17) to exceed the Lawson condition, one needs $M_s = 5$ if the temperature is 12 keV. Thus, from a transport viewpoint, high Mach numbers are again desirable.

The equations (12) and (13) constitute a simple transport model for the system that is qualitative at best. We have made no attempt to model profile effects or to account for detailed values of numerical prefactors in the various formulas. Clearly, the classical transport assumption needs to be experimentally demonstrated. With this in mind, we have calculated a reactor point as follows: Consider a system such as Fig. 2 where a is the plasma width at midplane, L is the axial extent of the plasma, R is the average major radius at the plasma midplane. Then, for $n = 0.6\times 10^{20}\,\mathrm{m}^{-3}$, $B = 2.6\,\mathrm{T}$, $a = 1.1\,\mathrm{m}$, $L/a = 20$, $R/a = 4$, and $P_{\mathrm{in}} = 3\,\mathrm{MW}$, we find $T = 13\,\mathrm{keV}$, $M_s = 6$, and $P_{\mathrm{fusion}} = 240\,\mathrm{MW}$. (All plasma parameters refer to averaged values at the midplane.) This corresponds to a maximum electric field at the midplane of 10 MV/m. We have made the assumptions that charge exchange, bremmstrahlung, and impurity radiation losses are negligible. Note that other external momentum sources—neutral beams or radiofrequency fields—could also be considered to maintain the electric field.

In the reactor point above, we have made the additional assumption that the α particles are not confined. Being energetic, these are not centrifugally confined. However, they will be mirror confined up to the scattering time into the loss cone. It can be calculated that the α's would then share a significant portion of their energy with the electrons before they scatter into the loss cone. For our system, however, it is not clear how much energy deposition by the α's is desirable. The system would always need input power to maintain the rotation and the same power then heats the plasma (α's probably cannot be used to transfer momentum). Any additional heating sources would lower the Mach number, which may not be desirable. In any case, the amount of α heating could be controlled by selecting the right mirror ratio.

D. MHD stability

For a configuration such as that of Fig. 2 to be viable as a fusion device, MHD stability is the key issue. This is particularly the case for Fig. 2 because it is immediately clear from classical mirror theory that this configuration is unstable to the interchange flute mode: in the absence of a toroidal magnetic field and the absence of rotation, the growth rate of the interchange, γ_{int}, has been calculated and scales as[13]

$$\gamma_{\mathrm{int}} \sim c_s/(L_p L)^{1/2}. \tag{18}$$

Here, L_p is the pressure scale size and L is the axial length of the system. Note that an elongated plasma is less unstable since elongation effectively reduces the average radius of curvature of the field lines.[14]

In the case of a centrifugally confined plasma, however, there is substantial rotation and rotation shear. It has become clear in recent years that velocity shear can suppress interchange-like modes.[15,16] While the shear stabilization idea has been broached much earlier,[17] recent experimental evidence[18] and numerical evidence[19,20] have corroborated recent theoretical results[16] that show that even the ideal MHD interchange mode can be stabilized by sufficient velocity shear. For a toroidal rotation and a purely poloidal magnetic field, the stability criterion can be schematically written as[16]

$$R d\Omega/dr > \gamma_{\mathrm{int}}[\ln(R_\mu)]^{1/2}, \tag{19}$$

where R_μ is a Reynolds number based on the geometric mean of the viscosity and the resistivity. Note now that the velocity shear acts on the short radial scale a; then, using $d/dr \sim 1/a$ in (19) and using (18), we may rewrite the stability criterion as[14]

$$M_s > [(a/L)\ln(R_\mu)]^{1/2}. \tag{20}$$

Condition (20) suggests that if one can rotate at supersonic speeds and take advantage of an elongated configuration, one could stabilize the flute interchange. This constitutes one of the two driving motivations of the centrifugal approach: high

Mach number flows not only give centrifugal confinement, they also stabilize the flute. In addition, we showed in Sec. II C that high Mach numbers are also a requirement to access the Lawson condition.

The ingredients of the above conclusion—velocity shear suppression, supersonic flow, elongation, etc.—have been extensively cross-checked and shown to hold up in several analytical and numerical calculations. The evidence supports the following qualitative conclusions: (1) high Mach numbers, ~4–5, would be required; (2) elongation would lower Mach number requirements; (3) there might be a residual wobble in that the velocity shear may not completely stabilize the flutes, especially if the Mach number does not get high enough or is clamped to a low value; (4) there is a possibility that the Kelvin–Helmholtz (KH) may be weakly unstable, on transport time scales. This evidence is detailed in the appendix. For now, the evidence suggests that a weak toroidal magnetic field may be required to suppress any residual flutes or the Kelvin–Helmholtz instability—the toroidal field will provide the requisite stabilization from magnetic shear. In addition, the system should be elongated.

III. THE MARYLAND CENTRIFUGAL TORUS, MCT

The major goal of the MCT experiment is to produce a plasma with supersonic toroidal rotation and to study the confinement and MHD stability of the system. In particular, we hope to achieve $M_s > 3$, enhanced axial localization of the plasma as illustrated by a substantial plasma pressure drop from the midplane to the end of the device, and stabilization of the MHD flute modes by velocity shear. Since MCT is inherently a device with large velocity shear, it is also an excellent experiment for a basic study of stabilization of instabilities by velocity shear.

A. Guidelines from theory and modeling

The Maryland Centrifugal Torus as designed will be a modest size, cost effective, and flexible experiment. The design has been substantially guided by the theoretical work described above. Of note, the following features have been incorporated into the design.

(i) A strong magnetic field, so that $\rho_i \ll a$. This ensures that the experiment will be in the MHD regime.
(ii) Sufficient voltage to allow high speeds, up to the Alfvén speed, to attain high Mach numbers, $M_s \sim 3-5$. High Mach flows are essential for all three aspects of equilibrium, stability, and transport.
(iii) High in–out excursion of the field lines, $R_2/R_1 \gg 1$. Here, R_2 is the outermost radius of a field line, R_1 is the radius of closest approach to the axis. As deduced from Eq. (11), this feature maximizes the axial pressure drop.
(iv) Elongated plasmas with $L/a \gg 1$. As mentioned, this enhances velocity shear efficacy and lowers Mach number requirements.
(v) Inclusion of a toroidal field, B_T, capability. It is possible there may be some residual convection from interchange modes or a weak Kelvin–Helmholtz: the toroidal field will provide magnetic shear to suppress such residual modes. In particular, since the convection is weak, not much toroidal field may be needed ($B_T \ll B_P$), although we plan conservatively for $B_T \sim B_P$.

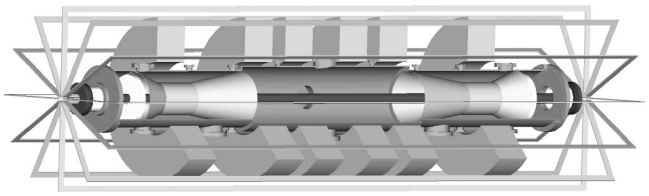

FIG. 4. A schematic cutaway of the MCT device. A poloidal (mirror) magnetic field is produced by the two high-field end coils and the four center section solenoid coils. The toroidal magnetic field is produced by 12 discrete coils, as shown. The tube running through the center of the vacuum vessel is the high-voltage core, which also carries the inner legs of the toroidal field coils. Insulators are shown in white. The double cone-shaped objects in the end sections (liners) serve the purpose of shaping the electrostatic potential. In operation the core is biased at high voltage with respect to the outer vessel. The outer diameter of the end and the solenoidal coils is 1 m.

The B_T capability is also important in the sense that it can act as an ''assist'' to attaining high Mach numbers—if the Mach numbers are low and there is significant residual convection, then the Mach number may be ''clamped'' at this level if the turbulence makes the momentum and heat confinement times equal. In that case, a toroidal field could help to suppress the turbulence just enough to lift the system to a higher Mach number operating regime wherein the confinement improves.

As discussed in Sec. II, a transport model has been developed. This model incorporates both fully ionized plasma effects as well as a variety of plasma/neutral interactions. The conclusions of the modeling are that in a small device such as MCT plasma momentum loss will probably be dominated by resonant charge exchange and the energy loss likely strongly influenced by charge exchange and radiation from higher Z impurities, especially oxygen. Given this expectation, the MCT design and plan includes significant efforts at surface conditioning, as will be described in more detail below.

Finally, a study of earlier experiments[2,3] shows clearly that the high voltage–insulator regions require concentrated effort and experimentation. For this reason MCT will incorporate a ''dual insulator'' configuration in which the plasma facing insulator (referred to as the baffle insulator in this paper) is separate from the high voltage, high vacuum insulator (see Fig. 4). More details are given below.

B. The MCT device

Figure 4 shows a schematic picture of the MCT device as currently designed. The major components are shown. The important subsystems are now discussed.

Axial Magnetic Field System: The main magnetic field will be produced by six identical high field air core coils configured in two groups: four coils for the central solenoid and two high field mirror end coils. Each group is powered by a separate power supply. The major features of this highly flexible system are as follows: The Central Solenoid will

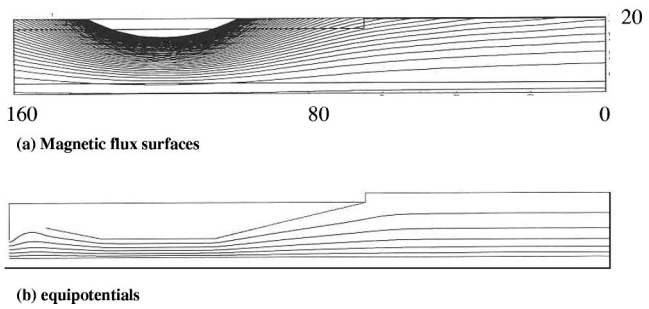

FIG. 5. (a) Magnetic field lines in the upper left quadrant of the *R,Z* plane for the $R_M=9.8$ mirror geometry. Scale markings are in cm. (b) Equipotentials for the corresponding liner geometry of Fig. 4; shown approximately to the same scale as (a).

allow $B\leqslant 0.7\,\mathrm{T}$ (continuous); the end coils will allow $B\leqslant 2.1\,\mathrm{T}$ (10 s switched dc); the system will thus allow mirror ratios, R_M, in the range 3–10.

In Fig. 5(a), we show magnetic flux contours for the high mirror ratio case, $R_M=9.8$. Good field line configurations have been obtained over the full mirror ratio range.

Toroidal Magnetic Field System: The pulsed toroidal field will be generated by 12 coils fabricated from a copper bar and driven by a pulsed electrolytic capacitor bank. The toroidal system produces $B_T\leqslant 0.2\,\mathrm{T}$ at $r=0.15\,\mathrm{m}$ (the center of the midplane plasma region) with a flat-top duration of approximately 10 ms.

Vacuum Vessel: The vessel will be fabricated from standard 304SS Conflat hardware to ensure ultrahigh vacuum capability, ease of design, and reasonable cost. Adequate diagnostic access is designed in, especially access for diagnosing the very important insulator region. At each end of the machine will be two six inch i.d. pumping ports. The inner port (closer to the midplane) is located between the high-field mirror coil and the solenoid region and will be used to pump the central plasma region. The outer pumping port will be located between the end of the device and the baffle insulator and it will be used to differentially pump the region where the high vacuum insulator resides, thus reducing the probability of breakdown in this region.

Central Core: This is a unique feature of MCT and provides the high-voltage ($\leqslant$20 kV) center electrode for the $\mathbf{E}\times\mathbf{B}$ discharge as well as carrying the central legs of the toroidal field coils. The core will be at high voltage, insulated from the main vessel and also insulated from the legs of the toroidal coils. Note that core insulation from the vessel occurs in a region at the machine ends completely shielded from the plasma. These high vacuum feedthrough insulators are distinct from the baffle insulating assemblies described below. The core may be run as an anode or a cathode.

Discharge Power Source: The discharge will be powered by a high-voltage capacitor bank. The pulsed power source is designed to allow disconnecting of the source from the plasma during a discharge to produce ''free wheeling'' decay of the rotating plasma or disconnecting the source but switching in a known resistance in the decaying circuit. These features are very useful for diagnosing the gross features of the plasma, including a measurement of the momentum confinement time. The circuit also includes a variable series inductor that allows lengthening the duration of the formation phase. The bank parameters are as follows: $V=11\,\mathrm{kV}$, $C=5.6$ millifarads, stored energy $E_C=0.34\,\mathrm{MJ}$. Ignitron tubes will be used for the various switching. We have estimated the discharge current required using our transport model and we have more than sufficient stored energy capability to provide a minimum flat-top pulse time of 5 ms. If required in later experiments the bank can easily be upgraded to 18 kV.

Shaped Liner: An optimum $\mathbf{E}\times\mathbf{B}$ device would have $\mathbf{E}$ perpendicular to $\mathbf{B}$ everywhere and indeed the plasma will force itself toward this situation. This implies that magnetic flux surfaces correspond to electric equipotentials and we have attempted to satisfy this over much of the system for the vacuum field so that the equipotentials begin at $t=0$ close to where we would like them to be during the discharge. To obtain this we have added shaped liners as electrode surfaces on each end of the device and the center of the core. We have used an electrostatic simulation code to evaluate our design and Fig. 5(b) shows equipotential lines corresponding to liner shapes needed for the high mirror ratio case of Fig. 5(a). In general, a different liner is required if the mirror ratio is changed substantially. The liners will be fabricated of stainless steel but in some regions will be composed of highly porous mesh to allow pumping or a diagnostic view through the liner.

Insulating Assemblies: Preventing the short circuiting of the electric field requires insulating assemblies at the ends of the device. These assemblies can take the form of simple insulating disks or more complicated arrays of electrically floating metallic rings that are insulated from each other. The insulating assemblies must hold off the applied voltage of $\leqslant$20 kV or so and not arc down in the presence of plasma. On MCT we have chosen a dual insulator concept wherein there are two insulators at each end. The one closer to the midplane is called the *baffle* insulator; it is the plasma facing component and it covers most of the area between the core and the outer vacuum vessel wall. The second insulator is at the end of the machine and is both a high voltage insulator and a high vacuum *feedthrough* for the high voltage. The baffle insulator shields the high vacuum feedthrough insulator from plasma bombardment, plasma ultraviolet radiation, and from metal coating from the plasma. MCT will also be differentially pumped in the region between the two insulators so that the neutral pressure in the vicinity of the high vacuum feedthrough will be considerably lower than in the central plasma region. These steps are designed to drastically reduce the probability of breakdown at the feedthrough insulator. We also note that in MCT the plasma facing baffle insulating assemblies will be located beyond the mirror throats where the *B* lines have expanded considerably. This allows the insulators to be larger and reduces the power density incident on the insulator and the electric field strength.

Preionization: Most previous rotating plasma experiments employed the applied electric field to break down and form the ionized plasma. While we will certainly explore this mode of operation because of its simplicity, MCT will also employ some version of preionization in the interest of mak-

ing the formation phase smoother and perhaps generate fewer impurities. We will begin with electron cyclotron heating (ECH) preionization that is well suited to the nonuniform B of the magnetic mirror geometry and has seen wide application in this configuration. It also allows nonintrusive preionization. Given our range of magnetic fields, X band ($\sim$3 cm wavelength) microwave radiation with a fundamental electron cyclotron resonance at $B \sim 0.3$ T is ideal and we will initially use the preionization source from the Maryland Spheromak. We will also explore other methods of preionization such as washer gun generated plasmas.[21]

Wall conditioning: Maintaining an acceptable level of neutrals (both hydrogen and heavier impurities) is vital to the success of the experiment. MCT will use ultrahigh vacuum components (hard seals) and turbomolecular and cryopump and we expect base pressures in the 1×10^{-7} Torr range or better. We will also employ wall conditioning to reduce recycling and impurity influx during a discharge. In particular, we will use (a) *electropolishing* of the major interior metal surfaces, especially the vacuum vessel, the core, and the shaped liner; (b) *bakeout* to 150 °C to remove much of the trapped water vapor, which will be accomplished by conventional resistive heaters on the vessel; (c) *titanium gettering* of the central region of the machine; (d) *discharge cleaning* with both hydrogen and helium. Implementation of these must, of course, be consistent with our insulator integrity.

From the above design, from considering previous experiments, as well as studies with the transport code, MCT is expected to operate in the following parameter ranges. For the design parameters $a \sim 0.1$ m, $L \sim 1.5$ m, $B = 0.2-2.0$ T, mirror ratio$=3-10$, fill pressure $\sim$1 mTorr, $V < 20$ kV, the expected plasma parameters are $n \sim 10^{19}-10^{20}$ m^{-3}, $T_e \sim T_i \sim 10-100$ eV, $a/\rho_i > 20$, $M_s \sim 3-6$.

The system will include flexibility in the magnetic field strength and mirror ratio, the addition of a toroidal field, as well as flexibility in the applied voltage and its rise time, and the fill pressure. The plasma density is not independently controlled but should be variable over some range. We will investigate two preionization approaches: ECH and gun or filament generated plasmas and will also experiment with static fill as well as gas puffing to establish density control and vary neutral density. The existence of a toroidal magnetic field gives us important extra flexibility in forming the equilibrium.

Large $\mathbf{E} \times \mathbf{B}$ flow and associated shear, manifest in the bulk of the plasma, are central underpinnings of this experiment. It would be useful to have active control of the potential and, thus, the velocity profile. MCT will have limited capability in this regard. The baffle insulator assemblies may take the form of a collection of metal rings, which may result in an altered profile. The rings could be connected by appropriately chosen resistors to alter the profile with respect to the floating case. In Ref. 3, these type of rings were externally biased at different potentials. While such profile control would be beyond the scope of the early MCT phases, it could be implemented in an upgrade phase. We note that experiments with toroidal momentum input on the DIII-D and Tokamak Fusion Test Reactor (TFTR) tokamaks showed that when momentum is deposited in the center of the plasma, the plasma flow relaxes under viscosity to a parabolic-type profile, indicating that the walls act as ''no-slip'' boundaries. The numerical simulations reported in Fig. 3 also demonstrated relaxation under viscosity to such profiles using no-slip boundary conditions. The same situation will likely prevail on MCT, that is, no-slip boundary conditions should result in a naturally sheared flow profile—MCT will be run for several expected momentum confinement times. For larger experiments, neutral beam or radiofrequency momentum drives can be imagined, as mentioned, with the possibility of some profile control. Finally, whether or not spontaneous transport barriers will arise in the MCT experiment is unknown.

To achieve our research goals, certain critical issues must be addressed and experimentally investigated. The most important of these are the following.

(1) The electric must be shown to penetrate the plasma. A direct measurement of the rotation speed is required to assess this.
(2) It must be determined that the equilibrium is stable to gross MHD instabilities. In this vein, it is important to note that determination of MHD stability is not as directly analogous to that conventionally done in tokamaks or RFPs (reversed field pinch) because the operative instability here is the interchange and not kink-tearing modes.
(3) It must be determined that the plasma is localized away from the mirror throats, as one would expect for strong centrifugal effects.
(4) The equilibrium must be maintained for at least several confinement times ($\sim$ a few milliseconds) to investigate steady-state and transport aspects.
(5) It would be desirable to ascertain evidence of any suppression of microinstabilities by velocity shear.

IV. SUMMARY

In this paper, we have assessed the plasma physics feasibility of centrifugally confined plasmas as a fusion scheme. We conclude that rotation at supersonic speeds, $M_s > 4-5$, will lead to good containment, keep the system MHD stable, iron out microturbulence, and allow a Lawson breakeven. These conclusions have been arrived at from a combination of analyis and numerical simulation.

The fusion device that emerges from optimizing over the plasma rotation ''knob'' features four advantages as a fusion reactor: (1) the system is steady state (all magnetic fields are generated by external coils); (2) there are no tokamak-type disruptions (there are no externally driven parallel currents and, so, no kink modes); (3) the cross-field transport may be classical (large velocity shear suppresses microturbulence and there are no banana orbits); (4) the coil configuration is relatively simple (little or no toroidal field is required, there is a long ''central cell'').

The MCT experiment, presently under construction, will be a modest size experiment to investigate some of the physics of centrifugal confinement. In particular, it will aim at obtaining stable MHD equilibria. To this end, the system will

feature elongation—to increase velocity shear efficacy—and a toroidal field capability—to provide an assist to MHD stability via magnetic shear.

APPENDIX: THEORETICAL RESULTS ON MHD STABILITY

Several analytic calculations and numerical simulations have been done to assess the velocity shear stabilization of MHD flute instabilities. We summarize the key results here.

(1) *Rayleigh–Taylor—Analysis*.[16] The classic Rayleigh–Taylor interchange instability in the presence of an external velocity shear was analyzed. For a linearly varying velocity profile, a complete analytic calculation is possible. A stability criterion was obtained from which (19) is directly deduced. This criterion is more pessimistic than that of Kuo,[22] by the logarithmic factor of Eq. (19). This is because Kuo's calculation is based on eigenmodes while Ref. 14 is done as an initial value problem. Since the underlying eigenmode equation is not a Sturm–Liouville system, an eigenmode analysis may not constitute the complete response. The criterion (19) is more optimistic than that of Lehnert,[17] who proposed velocity shear stabilization very early on. Lehnert's conclusion was based on a local analysis, which is a good indicator of the trend but is superceded by Kuo's eigenmode analysis.

(2) *Rayleigh–Taylor—Nonlinear simulation*.[19] A nonlinear, numerical simulation was done to confirm the above analytic results. Qualitative features in agreement with the prediction from (1) above were obtained. In particular, for large enough applied velocity shear, complete laminarity was obtained in the density profile.

(3) *Effect of elongation*.[14] An analytic study was done to assess the effect of elongation. We considered a Z-pinch equilibrium (axially symmetric cylinder with purely azimuthal magnetic field) with a rectangularly shaped cross section. Sausage modes were analyzed with an imposed axial sheared flow. A stability criterion analogous to (1) above was obtained, which clearly showed that Mach number requirements went down as $(a/L)^{1/2}$, as in Eq. (19).

(4) *Velocity shear stabilization of Z pinch*.[20] A nonlinear numerical experiment was done to try and stabilize a Z pinch with an axial flow forced with no-slip boundary conditions at the walls. Z pinches are unstable to both interchange and kink modes. Stabilization was observed. However, at a given central Mach number, there was a residual wobble in the system. The size of the wobble decreased as the Mach number was increased, At a Mach number of about 5, the laminar pressure profile was recovered in more than 95% of the volume—a small, insignificant residual wobble remained in the center of the discharge.

(5) *Stability of Dean flow*.[23] In studies (1)–(4) above, we have dealt only with systems without centrifugal force. While shear in angular frequency of rotation is stabilizing, the centrifugal force itself is destabilizing, in that it adds to the effective gravity outward, as can be deduced from Fig. 2. To assess these countertendencies, we performed an analytic stability calculation for a system very similar to that of Fig. 2, but, for simplicity, we assumed a straight uniform axial field (i.e., only the solenoidal field). This system, referred to in fluid dynamics as Dean flow, contains the ingredients of rotation shear as well as destabilization from the centrifugal force. We found that the centrifugal force acts only on density gradients: if there are no density gradients, the conclusion of criterion (19) holds. If there are density gradients, one could still stabilize interchanges, but at somewhat higher Mach numbers. However, making the system have a large aspect ratio would bring down the Mach number requirements, analogous to the advantages of elongation.

(6) *The Kelvin–Helmholtz instability*.[23,14,24] It is well known that curvature in the flow profile can destabilize the Kelvin–Helmholtz. This instability, however, is weakly growing if the flow profile does not have an inflection point, which is quite likely the case for the flow profiles one may expect from a system such as in Fig. 2 (this result is known as the Rayleigh Inflection Theorem[25,23,14]). In particular, the growth rate scales as a fractional power of the inverse Reynolds number times Ω. In addition, the band of unstable wave numbers in the toroidal direction goes to lower and lower values with increasing Reynolds number, to a point that they may be out of range of the allowable wavelengths that could fit into a toroid. The KH is thus not a major concern—if necessary, a relatively weak toroidal field could be added to suppress any slowly growing modes.

(7) Work is in progress to extend the analysis and numerical simulations reported above to the complete geometry of Fig. 1. Preliminary analytical results[26] are in agreement with the Dean Flow and elongation calculations reported in (3) and (5). Preliminary numerical results exhibit stability with a small residual wobble at modest Mach numbers.

ACKNOWLEDGMENTS

We have benefited greatly from useful conversations with Dr. T. M. Antonsen, Jr., Dr. A. W. DeSilva, Dr. R. J. Goldston, Dr. S. K. Guharay, Dr. P. Heitzenroeder, Dr. B. Lehnert, Dr. R. Majeski, Dr. J. Rodgers, Dr. P. Valanju, and Dr. V. Volosov.

This work was supported by the Department of Energy.

[1] K. Boyer, J. E. Hammel, C. L. Longmire, D. Nagle, R. Ribe, and W. B. Riesenfeld, *Proceedings of the 2nd International Conference on Peaceful Uses of Atomic Energy* (United Nations, Geneva, 1958), Vol. 31, p. 319.
[2] B. Lehnert, Nucl. Fusion **11**, 485 (1971).
[3] G. F. Abdrashitov, A. V. Beloborodov, V. I. Volosov, V. V. Kubarev, Y. S. Popov, and Y. N. Yudin, Nucl. Fusion **31**, 1275 (1991).
[4] A. B. Hassam, Comments Plasma Phys. Control. Fusion **18**, 275 (1997).
[5] R. F. Ellis, A. B. Hassam, S. Guharay, S. Messer, and B. R. Osborn, Bull. Am. Phys. Soc. **44**, 48 (1998).
[6] E. Hamieri, Phys. Fluids **26**, 230 (1983).
[7] A. B. Hassam, Nucl. Fusion **36**, 707 (1996).
[8] B. R. Osborn, R. F. Ellis, and A. B. Hassam, Bull. Am. Phys. Soc. **43**, 1719 (1998).
[9] D. J. Griffiths, *Introduction to Electrodynamics* (Prentice–Hall, Englewood Cliffs, NJ, 1989).

[10]R. J. Goldston and P. H. Rutherford, *Introduction to Plasma Physics* (Institute of Physics Publishing, Philadelphia, 1995).
[11]S. I. Braginskii, Rev. Plasma Phys. **1**, 205 (1965).
[12]V. P. Pastukhov, Nucl. Fusion **14**, 3 (1974).
[13]J. P. Freidberg, *Ideal Magnetohydrodynamics* (Plenum, New York, 1987).
[14]A. B. Hassam, Phys. Plasmas **6**, 3772 (1999).
[15]H. Biglari, P. H. Diamond, and P. W. Terry, Phys. Fluids B **2**, 1 (1990).
[16]A. B. Hassam, Phys. Fluids B **4**, 485 (1992).
[17]B. Lehnert, Phys. Fluids **9**, 1367 (1966).
[18]R. Groebner, Phys. Fluids B **5**, 2343 (1993).
[19]A. B. Hassam, T. M. Antonsen, J. F. Drake, P. N. Guzdar, C. S. Liu, D. R. McCarthy, and F. L. Waelbroeck, Phys. Fluids B **5**, 2519 (1993).
[20]S. DeSouza-Machado, A. B. Hassam, and R. Sina, Phys. Plasmas **7**, 4632 (2000).
[21]A. G. Fiksel, A. F. Almagri, D. Craig, M. Tida, S. C. Prager, and J. Sarff, Plasma Sources Sci. Technol. **5**, 78 (1996).
[22]S. P. Kuo, Phys. Fluids **6**, 195 (1963).
[23]A. B. Hassam, Phys. Plasmas **6**, 3738 (1999).
[24]E. P. Velikhov, Sov. Phys. JETP **36**, 848 (1959).
[25]S. Chandrasekhar, *Hydrodynamic and Hydromagnetic Stability* (Oxford University Press, Oxford, England, 1961).
[26]D. Goel and A. B. Hassam, Bull. Am. Phys. Soc. **45**, 211 (2000).